Revision 1

Optical properties of siderite ($FeCO_3$) across the spin transition: Crossover to iron-rich carbonates in the lower mantle

Sergey S. Lobanov[1,2,*], Alexander F. Goncharov[1,3] and Konstantin D. Litasov[2,4]

[1]Geophysical Laboratory, Carnegie Institution of Washington, 5251 Broad Branch Road, NW, Washington DC 20015. USA

[2]V.S. Sobolev Institute of Geology and Mineralogy, Russian Academy of Science, Siberian Branch, Koptyuga pr. 3, Novosibirsk 630090, Russia

[3]Center for High Energy Matter in Extreme Environments and Key Laboratory of Material Physics, Institute of Solid State Physics, Chinese Academy of Sciences, 350 Shushanghu Road, Hefei, Anhui 230031, China

[4]Novosibirsk State University, 2 Pirogova Street, Novosibirsk 630090, Russia

[*]e-mail: slobanov@carnegiescience.edu, tel: +1(202)6006476

ABSTRACT

Upper mantle carbonates are thought to be iron-poor and magnesium-rich. However, at lower mantle conditions spin-pairing transitions in iron-bearing phases may trigger iron redistribution between the minerals. Here, using visible and near infrared absorption measurements, we examine the siderite crystal field up to 65 GPa. Optical spectrum of siderite at 1 bar has an absorption band at 10325 cm^{-1} corresponding to the crystal field splitting energy (10Dq) of ferrous iron in an octahedral field. This band intensifies and blue-shifts (86 cm^{-1}/GPa) with pressure, but disappears abruptly at 44 GPa signaling the spin transition. Simultaneously, a new absorption band centered at 15629 cm^{-1}

(88 cm^{-1}/GPa) appears in the spectrum. Tanabe-Sugano diagram analysis allowed assigning the observed absorption bands to $^5T_{2g} \rightarrow {}^5E_g$ and $^1A_{1g} \rightarrow {}^1T_{1g}$ electronic transitions in high- and low-spin siderite, respectively. Similarly, we evaluate the crystal field splitting energy of low-spin siderite 10Dq = 17600 cm^{-1} (45 GPa), as well as the Racah parameters B = 747 cm^{-1} and C = 3080 cm^{-1}. We find that the crystal field stabilization energy (CFSE) of ferrous iron in low-spin siderite (45700 cm^{-1} at 45 GPa) is an order of magnitude higher than that in the high-spin phase (4130 cm^{-1} at 1 bar). From the derived CFSE values we estimate the iron-partitioning coefficient for the carbonate-perovskite system and show that low spin carbonates are iron-rich and magnesium-poor. We also show that the color of siderite is governed by the $^1A_g \rightarrow {}^1T_{1g}$ absorption band and the Fe-O charge transfer.

Keyword: crystal field, high pressure, crystal chemistry, Tanabe-Sugano diagram, iron partitioning.

INTRODUCTION

Carbonates are involved in the deep carbon cycle with subduction being the major process in transportation of carbon to the mantle (Dasgupta and Hirschmann, 2010; Dobretsov and Shatskiy, 2012). Chemical interaction of Ca-rich carbonates with silicate minerals in subducting slabs ultimately results in the formation of iron-bearing magnesite (Biellmann et al., 1993; Grassi and Schmidt, 2011; Litasov, 2011; Seto et al., 2008). Magnesite ($MgCO_3$) is isostructural with siderite ($FeCO_3$) with a continuous range of compositions established for natural and synthetic samples (Boulard et al., 2012; Rividi et al., 2010; Shatskiy et al., 2014). Laboratory experiments (Fiquet et al., 2002; Isshiki et al., 2004), together with findings of carbonates as inclusions in transition zone and lower mantle diamonds (Brenker et al., 2007; Bulanova et al., 2010), indicate that Mg,Fe-bearing carbonates may withstand high-pressure high-temperature conditions of subducting slabs, penetrate into the lower mantle, and experience structural transformations (Boulard et al., 2011;

Mao et al., 2011; Oganov et al., 2013; Skorodumova et al., 2005). If so, the electronic structure of iron in lower mantle carbonates may undergo a high-spin (HS) to low-spin (LS) transformation resulting in abrupt changes of carbonate physical properties.

The spin transition in siderite was first reported to occur at approximately 50 GPa by Mattila et al. (2007) who employed x-ray emission spectroscopy to measure the spin state of iron in siderite upon compression. Subsequently, the structures of HS and LS siderite were studied by synchrotron x-ray diffraction, and the spin transition pressure was established to be at 43-49 GPa (Lavina et al., 2009; Lavina et al., 2010b). Discontinuities in vibrational properties over the spin transition were revealed by Raman spectroscopy; it was found that the Raman shift of lattice modes increases abruptly, whereas C-O symmetric stretching vibration softens at the spin transition pressure indicating a collapse of the FeO_6 octahedra (Farfan et al., 2012; Lin et al., 2012). This is in agreement with the structural model of HS to LS transformation, where the atomic displacements upon the spin transition do not result in a space-group change, and the symmetry of LS siderite is the same as the HS phase (Lavina et al., 2010b). Elastic constants have been reported for a wide range of magnesite-siderite solid solutions both for the HS and LS states (Lavina et al., 2009; Lavina et al., 2010a; Lavina et al., 2010b; Lin et al., 2012; Litasov et al., 2013; Liu et al., 2014). It was established that the LS phase is denser and has a higher bulk modulus than HS siderite (Lavina et al., 2009; Lin et al., 2012; Liu et al., 2014). Overall, the pressure-induced spin transition of iron-bearing carbonates is well characterized by a number of experimental techniques. Likewise, theoretical modelling of siderite under pressure reproduces the spin transition at pressures in agreement with the experimentally-derived ones (Ming et al., 2012; Shi et al., 2008).

Discontinuities in the physical properties are accompanied by color changes from colorless (HS) to green (LS) and red (LS) as pressure is increased (Lavina et al., 2009). As electrons rearrange on the *d*-orbitals upon the spin transition, the energy separation between the ground and excited

electronic states of HS and LS is different (Burns, 1993); thus the apparent change in color is not unexpected. In siderite, iron is located in FeO_6 octahedrons and the degeneracy of five *d* orbitals is broken by the crystal field to three t_{2g} (lower in energy) and two e_g (higher in energy) orbitals (Ballhausen, 1962; Figgis, 1966). The ground state electronic configuration of HS ferrous iron is $^5T_{2g}$ (Burns, 1993), with five of the *d* electrons spread among *d* orbitals with parallel spins in accordance with the Hund's first rule, and the sixth *d* electron paired to the t_{2g} level. The ground state electronic configuration of LS ferrous iron is $^1A_{1g}$, with all electrons located on the t_{2g} orbitals (Burns, 1993). The electronic structures of HS and LS Fe^{2+} can be found elsewhere (e.g. Badro et al., 2003; Burns, 1993; Li et al., 2004). The energy gap between the t_{2g} and e_g orbitals is termed crystal field splitting energy (10Dq), and it always increases with pressure as the metal-oxygen distance decreases (Ballhausen, 1962; Burns, 1993; Drickamer and Frank, 1973; Figgis, 1966). Crystal field effects are now well known to contribute to bulk thermodynamic properties of materials and may affect chemical equilibrium between coexisting Fe-bearing phases (Badro et al., 2003; Crispin and Van Orman, 2010; Prescher et al., 2014). However, no data is currently available on the siderite crystal field splitting energy. In this paper we report the results of visible and near infrared (IR) spectroscopy of siderite single crystals in the 0-72 GPa pressure range. The measurements allowed us to characterize the energy separation between t_{2g} and e_g orbitals of ferrous iron in HS and LS siderite up to 65 GPa, evaluate crystal field contributions to thermodynamic properties of iron-bearing carbonates, and estimate the effect of spin transition on the carbonate iron content in the lower mantle.

EXPERIMENTAL METHODS

Chemically homogeneous siderite (Fig. 1) from Panasqueira tungsten mine, Covilhã, Castelo Branco, Portugal (mineralogical collection of Tohoku University Museum of Natural History) with a composition $Fe_{0.95},Mn_{0.05}CO_3$ was used in this study. Calcium, magnesium and other impurities total

content is less than 1 at% according to the electron microprobe analyses performed in the Geophysical Laboratory using a JEOL JSM-6500F field emission scanning electron microscope. Cleaved rhombohedral single crystals (typically 30 x 50 x 10 μm^3) were loaded in diamond anvil cells with culets of 200 or 300 μm in diameter. Holes of 100-200 μm in diameter were drilled in the center of rhenium gaskets and served as sample containers. Neon was used as a pressure medium. Pressure was determined by the ruby fluorescence method (Mao et al., 1978).

Optical properties of natural siderite were measured in UV-visible and near IR absorption spectral ranges up to 72 GPa. A fiber-coupled halogen-deuterium lamp served as a light source for optical measurements. The light was focused to a 50 μm spot on the samples and a 20 μm central portion of the transmitted radiation was selected by a confocal aperture. The light is transported by an all-reflective microscope with relay optics and projected on the entrance slit of the UV-vis and IR spectrometers. Spectra were collected in 9000-25000 cm^{-1} range using a 300 grooves/mm grating of an Acton Research Corporation Spectra Pro 500-i CCD spectrometer sensitive in UV-vis. Near IR absorption was collected for 512 scans with a Varian Resolution Pro 670-IR spectrometer using a quartz beam splitter in the 3000-10000 cm^{-1} spectral range with 4 cm^{-1} resolution. The microscope setup was previously described in detail (Goncharov et al., 2009). The sample absorbance was calculated as $A(\nu) = -\log_{10}(I_{sample}/I_{reference})$, where I_{sample} is the intensity of light transmitted through the sample, and $I_{reference}$ is the intensity of the radiation passed through the pressure medium. We neglected the light reflection from the sample as it is less than 4% and is comparable to the other experimental uncertainties (Goncharov et al., 2009). All absorption spectra were collected at room temperature. Linear baseline subtraction preceded the deconvolution of absorption bands into the Voigt functions. The two sigma uncertainty of the band's spectral position was within ± 200 cm^{-1}.

RESULTS AND DISCUSSION

Absorption spectra of high-spin siderite

A weak and broad absorption band centered at 10325 cm^{-1} can be observed at 1 bar (Fig. 2). We assign this band to the $^5T_{2g} \rightarrow {}^5E_g$ electronic transition as it is the only spin-allowed transition of the $^5T_{2g}$ ground state (Burns, 1993). This assignment provides the crystal field splitting energy of *d*-orbitals of Fe^{2+} in octahedral crystal field ($10Dq^{HS}$) at 1 bar. The energy of 10325 cm^{-1} is typical for the energy gap between t_{2g} and e_g orbitals of Fe^{2+} ions in octahedral crystal field. For example, 10Dq values for ferropericlase and ringwoodite at 1 bar were estimated to have energies of approximately 10850 and 10470 cm^{-1} respectively (Keppler and Smyth, 2005; Keppler et al., 2007). The shape of the absorption band is quite symmetrical and only one maximum can be observed; thus, FeO_6 octahedra in HS siderite can be considered as non-distorted. Absorption spectra of HS siderite measured at 0-43 GPa allowed tabulating $10Dq^{HS}$ values (Table 1). Expectedly, application of pressure increases the splitting between t_{2g} and e_g orbitals and blue-shifts the crystal field band (Fig. 3). The pressure shift is approximately linear with $d10Dq^{HS}/dP$ = 86 cm^{-1}/GPa. At the spin transition pressure the increased $10Dq^{HS}$ equals to the spin pairing energy: $10Dq=\Pi=2.5B+4C\approx19B$ (Hauser, 2004), where Π is the spin pairing energy, B and C are the Racah parameters of electron-electron repulsion. Accordingly, we get the Racah parameters B and C for Fe^{2+} in octahedral crystal field in HS siderite as B = 747 cm^{-1} and C = 3080 cm^{-1}. These values closely resemble $B^{VI}(Fe^{2+}) \sim 500$ cm^{-1} inferred from magnesiowustite optical absorption spectra in the proximity of HS to LS transition (Goncharov et al., 2006). Also, Gavriliuk et al. (2004) have reported similar values of B = 680 cm^{-1} and C = 3150 cm^{-1} for ferric iron in the octahedral crystal field of $FeBO_3$.

The increase in overall absorption from 0 to 44 GPa is small and HS siderite remains visually colorless and transparent. However, at 39 GPa a rise in absorption is evident at frequencies higher than 22500 cm^{-1}. We assign this band to Fe-O electron transfer in FeO_6 octahedra, as the position, intensity, and pressure-induced red-shift of this absorption edge are typical for metal-oxygen charge transfer transitions (Burns, 1993; Goncharov et al., 2006; Mao and Bell, 1972).

Absorption spectra of low-spin siderite

A green domain appeared in siderite single crystal at 44 GPa signaling the spin transition has started (Fig. 4). We attribute the presence of colorless (HS) and green (LS) domains of siderite in the sample to the presence of pressure gradients across the single crystal. This observation indicates that at room temperature the spin transition in pure siderite occurs in a very narrow pressure range (44±1 GPa). Previous estimations based on carbonate samples with variable iron content (0.12 to 0.87 Fe in formula unit) have reported spin transition pressures between 43-49 GPa (Farfan et al., 2012; Lavina et al., 2009; Lavina et al., 2010a; Lin et al., 2012; Liu et al., 2014; Nagai et al., 2010).

Absorption spectra of HS and LS siderite are very different. A significant increase in overall optical absorption of LS siderite (Fig. 2) accounts for the dramatic color changes over the spin transition. At 45.5 GPa, a new sharp absorption band can be observed at 15629 cm^{-1} (dv/dP = 88 cm-1/GPa). At the same time, the crystal field band observed in HS siderite is no longer present in the absorption spectra implying that the newly formed band is similar in nature to that in HS siderite; thus, it is related to *d-d* transitions. The ground state electronic configuration of LS Fe^{2+} in octahedral site is $^1A_{1g}$ with five spin-allowed *d-d* transitions (Burns, 1993). We assign the observed absorption band to the $^1A_g \rightarrow {}^1T_{1g}$ transition, as it is the lowest in energy out of all spin-allowed transitions, with the rest occurring at much higher energies (Fig. 5). The previously determined Racah parameter B permits plotting the absorption energies of this band on the Tanabe-Sugano diagram for a d_6 ion in octahedral crystal field, which in turn allows estimating the $10Dq^{LS}$ values in the LS state as schematically shown in Figure 5. Alternatively, the crystal field splitting energy has inverse fifth-power dependency on the metal-oxygen distance (Burns, 1993), offering another way to evaluate $10Dq^{LS}$: $\frac{10Dq^{LS}}{10Dq^{HS}} \approx \left(\frac{r_{HS}}{r_{LS}}\right)^5$, where r_{HS} and r_{LS} are the Fe-O bond distances in FeO_6 octahedra in HS and LS siderite respectively. Using the spectroscopically determined $10Dq^{HS}$ and

previously reported Fe-O distances for HS and LS siderite (Lavina et al., 2010b) we solved the proportion for $10Dq^{LS}$ at 45.5, 48.5, 52, and 57 GPa (Table 1). Two independently constrained $10Dq^{LS}$ values are in fair agreement (Fig. 3) indicating that the main absorption band observed in the spectra of LS siderite indeed belongs to $^1A_{1g} \rightarrow {}^1T_{1g}$ transition. The magnitude of $^1A_g \rightarrow {}^1T_{1g}$ absorption in LS siderite is much higher compared to $^5T_{2g} \rightarrow {}^5E_g$ in the HS phase. Such intensification may result from a relaxing of the Laporte selection rule, which states that electron transitions between orbitals with equal parity are forbidden. The selection rule may be lifted if FeO_6 clusters of LS phase get distorted or vibronic coupling occurs (Burns, 1993).

According to the Tanabe-Sugano diagram, the energy separation between the two lowest in energy excited states in LS siderite ($^1T_{1g}$ and $^1T_{2g}$) is approximately 11*B* (Fig. 5); thus, the energy of the $^1A_g \rightarrow {}^1T_{2g}$ transition can be estimated as approximately 23850 cm^{-1} at 45.5 GPa. However, this band is likely hidden by the high-frequency absorption edge, which is Laporte allowed; therefore it is much more intense. It is worth noting that no spin-forbidden transitions were observed in the studied spectral range, as the spectral positions of the $^1A_{1g} \rightarrow {}^3T_{1g}$, $^1A_{1g} \rightarrow {}^3T_{2g}$, and $^1A_{1g} \rightarrow {}^5T_{2g}$ transitions should be in the 8500-14100 cm^{-1} range as inferred from the Tanabe-Sugano diagram analysis (spin-forbidden transitions are not shown in Fig. 5). This is why we do not expect that the divalent manganese impurity (<5 at%) of our siderite samples significantly contributes to the absorption spectra as the ground state of HS Mn^{2+} ($^6A_{1g}$) has no spin-allowed transitions (Burns, 1993), and the HS configuration is stable up to at least 54 GPa (Farfan et al., 2013).

The energy of metal-oxygen charge transfer absorption also shows a clear discontinuity upon the HS to LS transition (Fig. 6). We have determined the positions of the absorption edge by fitting the spectra and assuming that the absorbance follows the energy dependence characteristic for a direct band gap: $A(\nu) \propto \sqrt{h\nu - E}$, where *A(ν)* is sample absorbance, *hν* is the photon energy, and *E* is the absorption edge energy. The position of absorption edge is shifted for about 2500 cm^{-1}

towards lower frequencies upon the HS to LS transformation, and is within the visible range at 45.5 GPa (Fig. 6). The color of LS siderite is governed by the interplay of the $^1A_g \rightarrow {}^1T_{1g}$ absorption band and the Fe-O charge transfer. Green color of LS siderite is due to the absorption minima at around 17500-20000 cm^{-1}. At P > 65 GPa siderite turns red, because of the overlap of the crystal field band with the absorption edge. Eventually, LS siderite turns black at pressures exceeding 71.5 GPa (Fig. 4) with Fe-O charge transfer absorption shifted to the near IR region.

Implications to carbonate crystal chemistry at lower mantle conditions

Spin pairing transitions may affect crystal chemistry of iron-bearing minerals (Badro et al., 2003; Lin et al., 2013). Iron content of carbonates in subducting slabs is controlled by partitioning coefficients *K(P,T)* between the carbonate phase and coexisting silicates (Kiseeva et al., 2013; Yaxley and Brey, 2004). Mg,Fe-perovskite (Pv) is the most abundant iron-bearing phase in a basaltic lithology at pressures exceeding 30 GPa (Hirose et al., 1999; Perrillat et al., 2006). Assuming no other Fe-bearing phases participate in the partitioning, the reaction can be written:

$$Fe_{Pv}^{2+} + Mg_{Carb}^{2+} = Fe_{Carb}^{2+} + Mg_{Pv}^{2+}.$$

At a given pressure and temperature, the partitioning coefficient is:

$$\ln K = \ln\left(\frac{Fe}{Mg}\right)_{Pv} - \ln\left(\frac{Fe}{Mg}\right)_{Carb} = -\frac{\Delta G(P,T)}{RT},$$

where ΔG is the Gibbs free energy of the reaction and R is the gas constant.

Crystal field stabilization energies (CFSE) contribute to the enthalpy terms of the Gibbs free energy and, as such, might be expected to affect the partitioning coefficient (Burns, 1993). CFSE values are 4Dq and 24Dq for HS and LS Fe^{2+} in an octahedral crystal field, respectively (Burns, 1993); whereas CFSE ≈ 6Dq for ferrous iron in the pseudo-dodecahedral crystal field of Mg,Fe-perovskite

(Keppler et al., 1994). Our optical absorption measurements yield over an order of magnitude increase in the Fe^{2+} CFSE in siderite, with a CFSE of 4130 cm^{-1} (HS phase, 1 bar) and 42181 cm^{-1} (LS phase, 45.5 GPa). In comparison, the increase of Fe^{2+} CFSE in Mg,Fe-perovskite is less pronounced and changes from approximately 4200 cm^{-1} (1 bar) to only 5100 cm^{-1} (46 GPa), as can be deduced from the absorption measurements by Goncharov et al. (2008), assuming all iron remains in the HS state. The difference between $CFSE_{Pv}$ and $CFSE_{Carb}$ gives us $\Delta CFSE = -445$ kJ/mol. To estimate the effect of spin transition on the partitioning coefficient one has to consider the electron-electron repulsion between paired electrons on the t_{2g} orbitals in LS siderite (5B+8C = 339 kJ/mole) (Lyubutin et al., 2013; Ovchinnikov, 2011). Likewise, the $P\Delta V$ contribution to the Gibbs free energy is -542 kJ/mole, accepting ΔV=10% at P = 45 GPa for the HS to LS transformation in pure $FeCO_3$ (Lavina et al., 2010b). Assuming no change in configurational entropy of carbonates across the spin transition, as well as $\Delta U^{HS}=\Delta U^{LS}$, where ΔU is the internal energy difference for the partitioning reaction between HS or LS carbonate and Mg,Fe-perovskite we can write:

$$lnK_{LS} - lnK_{HS} = \frac{P\Delta V + \Delta CFSE - 5B - 8C}{RT}$$

, where lnK_{LS} and lnK_{HS} are the logarithmic partitioning coefficients for the considered partitioning reaction, B and C are the Racah parameters. At 45 GPa and 2500 K we get $lnK_{LS} = -31.2 + lnK_{HS} = -29$, accepting $lnK_{HS} = 2.2$ (Stagno et al., 2011). Strongly negative values of lnK_{LS} suggest the composition of LS carbonates in equilibrium with Mg,Fe-perovskite is close to pure $FeCO_3$. However, the change in carbonate chemical composition with depth is likely to be gradual, because of the temperature-induced broadening of the spin transition pressure range (Lin et al., 2007; Liu et al., 2014; Lyubutin et al., 2013).

Acknowledgments

This study was supported by Deep Carbon Observatory and Ministry of Education and Science of Russian Federation (No 14.B25.31.0032). S.L. and A.F.G. would like to acknowledge the support from NSF EAR 1015239, EAR-1128867 and Carnegie Institution of Washington. We also thank N. Holtgrewe, V. V. Struzhkin, S.G. Ovchinnikov, and K. L. Crispin for valuable comments on the manuscript. J. Armstrong is thanked for the help in analyzing the carbonate chemical composition.

Tables

Table 1. *Position and assignment of the main absorption band in HS and LS siderite.*

High-spin	P, GPa	Absorption, cm^{-1}	FWHM, cm^{-1}	Electronic transition	$10Dq^{LS}$, cm^{-1}		CFSE, cm^{-1}
					Tanabe-Sugano	$10Dq^{HS}*(r_{HS}/r_{LS})^5$	
	0	10325	4241	$^5T_{2g} \rightarrow {}^5E_g$	–	–	4130
	25	12256	4295	$^5T_{2g} \rightarrow {}^5E_g$	–	–	4902
	28	12860	3963	$^5T_{2g} \rightarrow {}^5E_g$	–	–	5144
	39	13532	3838	$^5T_{2g} \rightarrow {}^5E_g$	–	–	5413
	43	14102	3627	$^5T_{2g} \rightarrow {}^5E_g$	–	–	5641
Low-spin	45.5	15629	2721	$^1A_{1g} \rightarrow {}^1T_{1g}$	17634	17517	42181
	45.5	15618	2879	$^1A_{1g} \rightarrow {}^1T_{1g}$			
	48.5	15973	2729	$^1A_{1g} \rightarrow {}^1T_{1g}$	18153	17844	43196
	52	16146	2587	$^1A_{1g} \rightarrow {}^1T_{1g}$	18301	18227	43834
	53	16079	2734	$^1A_{1g} \rightarrow {}^1T_{1g}$			
	57	16672	2560	$^1A_{1g} \rightarrow {}^1T_{1g}$	18819	18871	45228
	62	17116	2674	$^1A_{1g} \rightarrow {}^1T_{1g}$	19318		
	65	17332	2522	$^1A_{1g} \rightarrow {}^1T_{1g}$	19451		

Note: $10Dq^{LS}$ (crystal field splitting energy in low-spin siderite) cannot be measured directly in experiment. We independently estimated these values based on the Tanabe-Sugano diagram analysis, as well as on the relation between the Fe-O bond length and $10Dq^{HS}$ (see text). CFSE stands for the crystal field stabilization energy. Standard deviation is < 100 cm^{-1} for the absorption position.

Figures

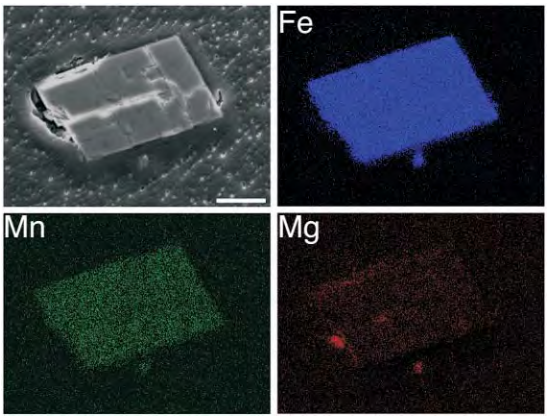

Figure 1. *Scanning electron image (top left) and corresponding elemental maps of Fe, Mn, and Mg of a representative siderite single crystal. The white scale bar corresponds to 10 μm.*

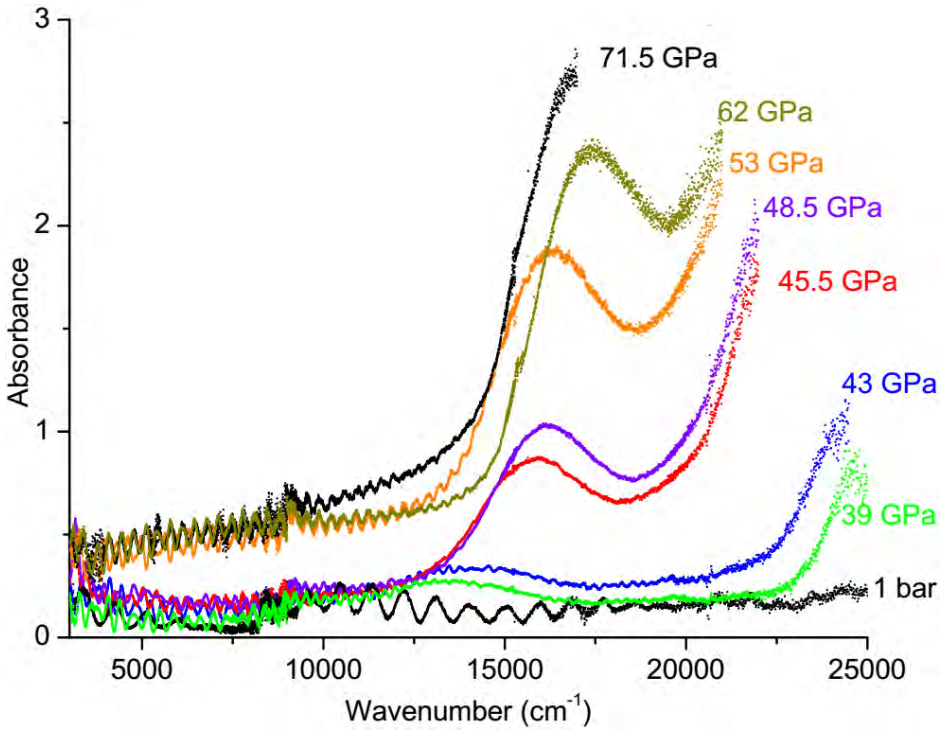

Figure 2. *Optical and near IR absorption spectra of siderite to 71.5 GPa. Low-frequency oscillations originate from multiple reflections between parallel sample surfaces.*

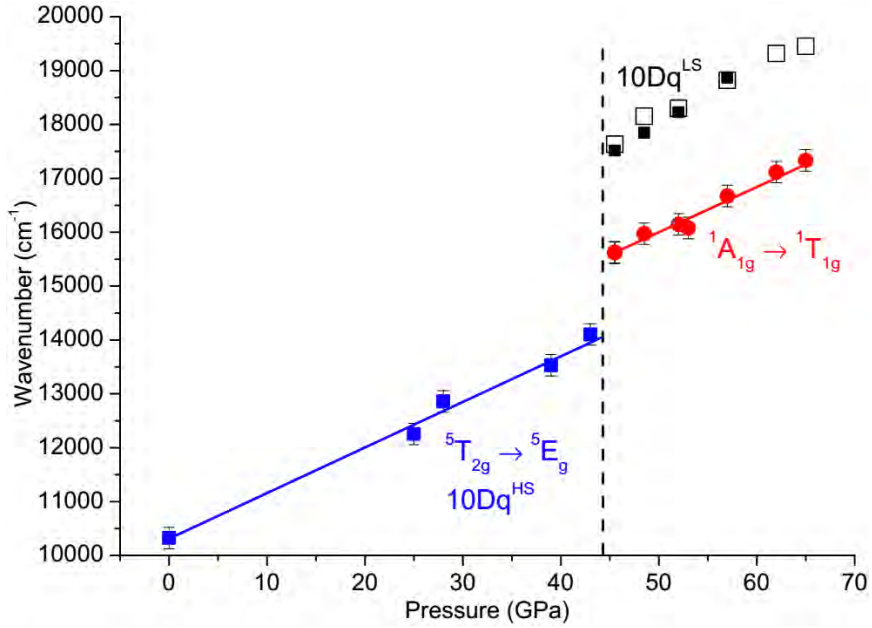

Figure 3. *Positions and assignment of absorption bands in HS and LS siderite. Blue squares and red circles represent the measured absorption bands. White and black squares approximate the* $10Dq^{LS}$ *values estimated with the Tanabe-Sugano diagram and through the inverse proportion with the* $(Fe\text{-}O)^5$ *bond distance, respectively. Vertical dashed line shows the spin transition pressure.*

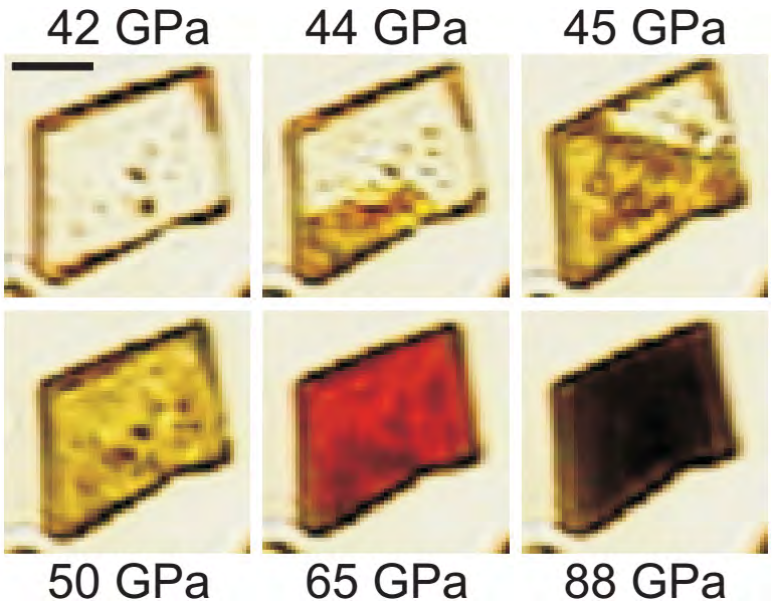

Figure 4. *Siderite color in HS (42 GPa), mixed HS and LS (44 and 45 GPa) and LS state (50, 65, and 88 GPa). The scale bar corresponds to 20 μm. Note the gradual growth of transient green LS domain at 44 and 45 GPa.*

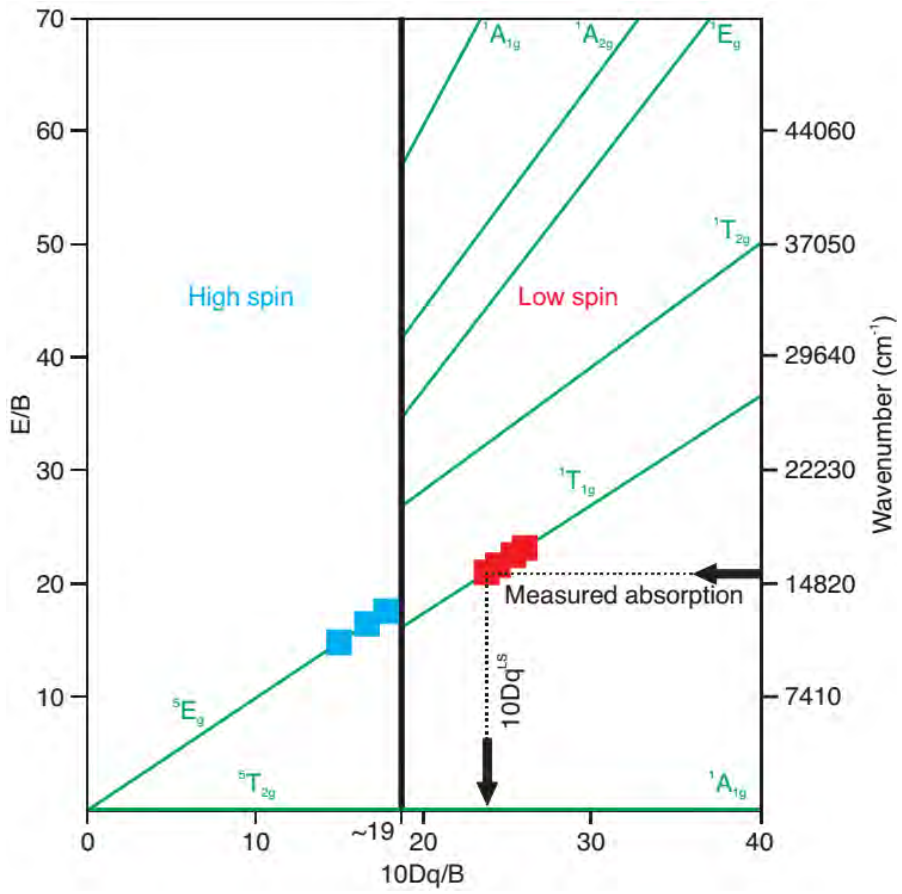

Figure 5. *The Tanabe-Sugano energy (E) level diagram for a d_6 ion in octahedral crystal field. Only spin-allowed electronic states are shown (green solid lines). Blue squares correspond to the $^5T_{2g} \rightarrow {}^5E_g$ transition in HS siderite at pressures of 0, 25, and 39 GPa. Red squares correspond to $^1A_{1g} \rightarrow {}^1T_{1g}$ absorption energies in LS siderite at 45.5, 52, 57, and 65 GPa. Spin transition occurs at $10Dq^{HS} \approx 19B$, shown by thick solid black line (B is the Racah parameter). Dotted lines show the procedure for $10Dq^{LS}$ estimation from the absorption band at 45.5 GPa.*

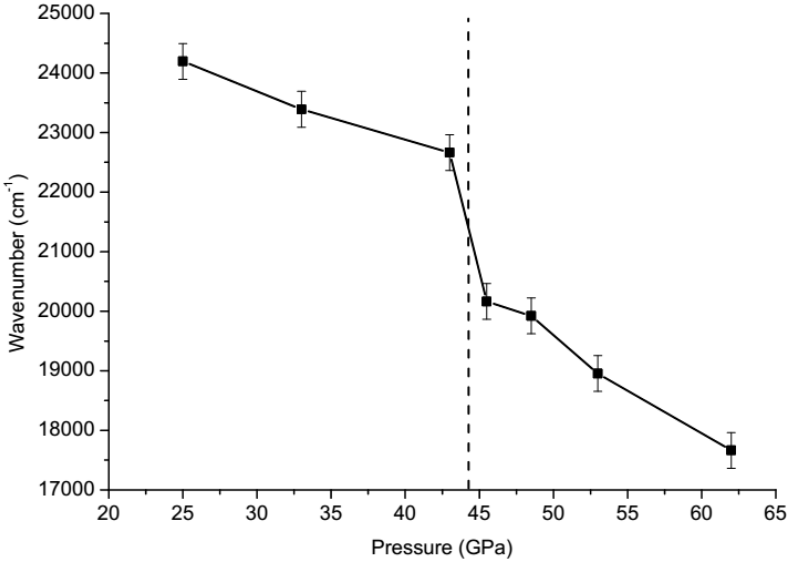

Figure 6. *Position of the absorption edge as a function of pressure. Vertical dashed line shows the spin transition pressure.*

Reference Cited

Badro, J., Fiquet, G., Guyot, F., Rueff, J.P., Struzhkin, V.V., Vanko, G., and Monaco, G. (2003) Iron partitioning in Earth's mantle: Toward a deep lower mantle discontinuity. Science, 300, 789-791.

Ballhausen, C.J. (1962) Introduction to ligand field theory, 298 p., McGraw-Hill, New York, U.S.A.

Biellmann, C., Gillet, P., Guyot, F., Peyronneau, J., and Reynard, B. (1993) Experimental-Evidence for Carbonate Stability in the Earth's Lower Mantle. Earth and Planetary Science Letters, 118, 31-41.

Boulard, E., Gloter, A., Corgne, A., Antonangeli, D., Auzende, A.L., Perrillat, J.P., Guyot, F., and Fiquet, G. (2011) New host for carbon in the deep Earth. Proceedings of the National Academy of Sciences of the United States of America, 108, 5184-5187.

Boulard, E., Guyot, F., and Fiquet, G. (2012) The influence on Fe content on Raman spectra and unit cell parameters of magnesite-siderite solid solutions. Physics and Chemistry of Minerals, 39, 239-246.

Brenker, F.E., Vollmer, C., Vincze, L., Vekemans, B., Szymanski, A., Janssens, K., Szaloki, I., Nasdala, L., Joswig, W., and Kaminsky, F. (2007) Carbonates from the lower part of transition zone or even the lower mantle. Earth and Planetary Science Letters, 260, 1-9.

Bulanova, G.P., Walter, M.J., Smith, C.B., Kohn, S.C., Armstrong, L.S., Blundy, J., and Gobbo, L. (2010) Mineral inclusions in sublithospheric diamonds from Collier 4 kimberlite pipe, Juina, Brazil: subducted protoliths, carbonated melts and primary kimberlite magmatism. Contributions to Mineralogy and Petrology, 160, 489-510.

Burns, R.G. (1993) Mineralogical applications of crystal field theory, 2nd ed., 551 p., Cambridge University Press, U.K.

Crispin, K.L., and Van Orman, J.A. (2010) Influence of the crystal field effect on chemical transport in Earth's mantle: Cr^{3+} and Ga^{3+} diffusion in periclase. Physics of the Earth and Planetary Interiors, 180, 159-171.

Dasgupta, R., and Hirschmann, M.M. (2010) The deep carbon cycle and melting in Earth's interior. Earth and Planetary Science Letters, 298, 1-13.

Dobretsov, N.L., and Shatskiy, A.F. (2012) Deep carbon cycle and geodynamics: the role of the core and carbonatite melts in the lower mantle. Russian Geology and Geophysics, 53, 1117-1132.

Drickamer, H.G., and Frank, C.W. (1973) Electronic transitions and the high pressure chemistry and physics of solids, 220 p., Chapman and Hall, U.K.

Farfan, G., Wang, S.B., Ma, H.W., Caracas, R., and Mao, W.L. (2012) Bonding and structural changes in siderite at high pressure. American Mineralogist, 97, 1421-1426.

Farfan, G.A., Boulard, E., Wang, S.B., and Mao, W.L. (2013) Bonding and electronic changes in rhodochrosite at high pressure. American Mineralogist, 98, 1817-1823.

Figgis, B.N. (1966) Introduction to ligand fields, 351 p., Interscience Publishers, New York, U.S.A.

Fiquet, G., Guyot, F., Kunz, M., Matas, J., Andrault, D., and Hanfland, M. (2002) Structural refinements of magnesite at very high pressure. American Mineralogist, 87, 1261-1265.

Gavriliuk, A.G., Trojan, I.A., Ovchinnikov, S.G., Lyubutin, I.S., and Sarkisyan, V.A. (2004) The mechanism of suppression of strong electron correlations in $FeBO_3$ at high pressures. Journal of Experimental and Theoretical Physics, 99, 566-573.

Goncharov, A.F., Struzhkin, V.V., and Jacobsen, S.D. (2006) Reduced radiative conductivity of low-spin (Mg,Fe)O in the lower mantle. Science, 312, 1205-1208.

Goncharov, A.F., Haugen, B.D., Struzhkin, V.V., Beck, P., and Jacobsen, S.D. (2008) Radiative conductivity in the Earth's lower mantle. Nature, 456, 231-234.

Goncharov, A.F., Beck, P., Struzhkin, V.V., Haugen, B.D., and Jacobsen, S.D. (2009) Thermal conductivity of lower-mantle minerals. Physics of the Earth and Planetary Interiors, 174, 24-32.

Grassi, D., and Schmidt, M.W. (2011) The Melting of Carbonated Pelites from 70 to 700 km Depth. Journal of Petrology, 52, 765-789.

Hauser, A. (2004) Ligand field theoretical considerations. Spin Crossover in Transition Metal Compounds I, 233, 49-58.

Hirose, K., Fei, Y.W., Ma, Y.Z., and Mao, H.K. (1999) The fate of subducted basaltic crust in the Earth's lower mantle. Nature, 397, 53-56.

Isshiki, M., Irifune, T., Hirose, K., Ono, S., Ohishi, Y., Watanuki, T., Nishibori, E., Takata, M., and Sakata, M. (2004) Stability of magnesite and its high-pressure form in the lowermost mantle. Nature, 427, 60-63.

Keppler, H., Mccammon, C.A., and Rubie, D.C. (1994) Crystal-Field and Charge-Transfer Spectra of $(Mg,Fe)SiO_3$ Perovskite. American Mineralogist, 79, 1215-1218.

Keppler, H., and Smyth, J.R. (2005) Optical and near infrared spectra of ringwoodite to 21.5 GPa: Implications for radiative heat transport in the mantle. American Mineralogist, 90, 1209-1212.

Keppler, H., Kantor, I., and Dubrovinsky, L.S. (2007) Optical absorption spectra of ferropericlase to 84 GPa. American Mineralogist, 92, 433-436.

Kiseeva, E.S., Litasov, K.D., Yaxley, G.M., Ohtani, E., and Kamenetsky, V.S. (2013) Melting and Phase Relations of Carbonated Eclogite at 9-21 GPa and the Petrogenesis of Alkali-Rich Melts in the Deep Mantle. Journal of Petrology, 54, 1555-1583.

Lavina, B., Dera, P., Downs, R.T., Prakapenka, V., Rivers, M., Sutton, S., and Nicol, M. (2009) Siderite at lower mantle conditions and the effects of the pressure-induced spin-pairing transition. Geophysical Research Letters, 36, L23306.

Lavina, B., Dera, P., Downs, R.T., Tschauner, O., Yang, W.E., Shebanova, O., and Shen, G.Y. (2010a) Effect of dilution on the spin pairing transition in rhombohedral carbonates. High Pressure Research, 30, 224-229.

Lavina, B., Dera, P., Downs, R.T., Yang, W.G., Sinogeikin, S., Meng, Y., Shen, G.Y., and Schiferl, D. (2010b) Structure of siderite FeCO3 to 56 GPa and hysteresis of its spin-pairing transition. Physical Review B, 82, 064110.

Li, J., Struzhkin, V.V., Mao, H.K., Shu, J.F., Hemley, R.J., Fei, Y.W., Mysen, B., Dera, P., Prakapenka, V., and Shen, G.Y. (2004) Electronic spin state of iron in lower mantle perovskite. Proceedings of the National Academy of Sciences of the United States of America, 101, 14027-14030.

Lin, J.F., Vanko, G., Jacobsen, S.D., Iota, V., Struzhkin, V.V., Prakapenka, V.B., Kuznetsov, A., and Yoo, C.S. (2007) Spin transition zone in Earth's lower mantle. Science, 317, 1740-1743.

Lin, J.F., Liu, J., Jacobs, C., and Prakapenka, V.B. (2012) Vibrational and elastic properties of ferromagnesite across the electronic spin-pairing transition of iron. American Mineralogist, 97, 583-591.

Lin, J.F., Speziale, S., Mao, Z., and Marquardt, H. (2013) Effects of the Electronic Spin Transitions of Iron in Lower Mantle Minerals: Implications for Deep Mantle Geophysics and Geochemistry. Reviews of Geophysics, 51, 244-275.

Litasov, K.D. (2011) Physicochemical conditions for melting in the Earth's mantle containing a C-O-H fluid (from experimental data). Russian Geology and Geophysics, 52, 475-492.

Litasov, K.D., Shatskiy, A., Gavryushkin, P.N., Sharygin, I.S., Dorogokupets, P.I., Dymshits, A.M., Ohtani, E., Higo, Y., and Funakoshi, K. (2013) P-V-T equation of state of siderite to 33 GPa and 1673 K. Physics of the Earth and Planetary Interiors, 224, 83-87.

Liu, J., Lin, J.F., Mao, Z., and Prakapenka, V.B. (2014) Thermal equation of state and spin transition of magnesiosiderite at high pressure and temperature. American Mineralogist, 99, 84-93.

Lyubutin, I.S., Struzhkin, V.V., Mironovich, A.A., Gavriliuk, A.G., Naumov, P.G., Lin, J.F., Ovchinnikov, S.G., Sinogeikin, S., Chow, P., Xiao, Y.M., and Hemley, R.J. (2013) Quantum critical point and spin fluctuations in lower-mantle ferropericlase. Proceedings of the National Academy of Sciences of the United States of America, 110, 7142-7147.

Mao, H.K., and Bell, P.M. (1972) Electrical conductiviy and the red shift of absorption in olivine and spinel at high pressure. Science, 176, 403-405.

Mao, H.K., Bell, P.M., Shaner, J.W., and Steinberg, D.J. (1978) Specific volume measurements of Cu, Mo, Pd, and Ag and calibration of the ruby R_1 fluorescence pressure gauge from 0.06 to 1 Mbar. Journal of Applied Physics, 49, 3276-3283.

Mao, Z., Armentrout, M., Rainey, E., Manning, C.E., Dera, P., Prakapenka, V.B., and Kavner, A. (2011) Dolomite III: A new candidate lower mantle carbonate. Geophysical Research Letters, 38, L22303.

Mattila, A., Pylkkanen, T., Rueff, J.P., Huotari, S., Vanko, G., Hanfland, M., Lehtinen, M., and Hamalainen, K. (2007) Pressure induced magnetic transition in siderite $FeCO_3$ studied by x-ray emission spectroscopy. Journal of Physics-Condensed Matter, 19, 386206.

Ming, X., Wang, X.L., Du, F., Yin, J.W., Wang, C.Z., and Chen, G. (2012) First-principles study of pressure-induced magnetic transition in siderite $FeCO_3$. Journal of Alloys and Compounds, 510, L1-L4.

Nagai, T., Ishido, T., Seto, Y., Nishio-Hamane, D., Sata, N., and Fujino, K. (2010) Pressure-induced spin transition in $FeCO_3$-siderite studied by X-ray diffraction measurements. Journal of Physics: Conference Series, 215, 012002.

Oganov, A.R., Hemley, R.J., Hazen, R.M., and Jones, A.P. (2013) Structure, Bonding, and Mineralogy of Carbon at Extreme Conditions. Reviews in Mineralogy & Geochemistry, 75, 47-77.

Ovchinnikov, S.G. (2011) Metallization and spin crossover in Magnesiowustite (Mg1-x Fe (x) O) at high pressures. Jetp Letters, 94, 192-196.

Perrillat, J.P., Ricolleau, A., Daniel, I., Fiquet, G., Mezouar, M., Guignot, N., and Cardon, H. (2006) Phase transformations of subducted basaltic crust in the upmost lower mantle. Physics of the Earth and Planetary Interiors, 157, 139-149.

Prescher, C., Langenhorst, F., Dubrovinsky, L.S., Prakapenka, V.B., and Miyajima, N. (2014) The effect of Fe spin crossovers on its partitioning behavior and oxidation state in a pyrolitic Earth's lower mantle system. Earth and Planetary Science Letters, 399, 86-91.

Rividi, N., van Zuilen, M., Philippot, P., Menez, B., Godard, G., and Poidatz, E. (2010) Calibration of Carbonate Composition Using Micro-Raman Analysis: Application to Planetary Surface Exploration. Astrobiology, 10, 293-309.

Seto, Y., Hamane, D., Nagai, T., and Fujino, K. (2008) Fate of carbonates within oceanic plates subducted to the lower mantle, and a possible mechanism of diamond formation. Physics and Chemistry of Minerals, 35, 223-229.

Shatskiy, A., Borzdov, Y.M., Litasov, K.D., Kupriyanov, I.N., Ohtani, E., and Palyanov, Y.N. (2014) Phase relations in the system $FeCO_3$-$CaCO_3$ at 6 GPa and 900-1700 °C and its relation to the system $CaCO_3$-$FeCO_3$-$MgCO_3$. American Mineralogist, 99, 773-785.

Shi, H., Luo, W., Johansson, B., and Ahuja, R. (2008) First-principles calculations of the electronic structure and pressure-induced magnetic transition in siderite $FeCO_3$. Physical Review B, 78, 155119.

Skorodumova, N.V., Belonoshko, A.B., Huang, L., Ahuja, R., and Johansson, B. (2005) Stability of the $MgCO_3$ structures under lower mantle conditions. American Mineralogist, 90, 1008-1011.

Stagno, V., Tange, Y., Miyajima, N., McCammon, C.A., Irifune, T., and Frost, D.J. (2011) The stability of magnesite in the transition zone and the lower mantle as function of oxygen fugacity. Geophysical Research Letters, 38, L19309.

Yaxley, G.M., and Brey, G.P. (2004) Phase relations of carbonate-bearing eclogite assemblages from 2.5 to 5.5 GPa: implications for petrogenesis of carbonatites. Contributions to Mineralogy and Petrology, 146, 606-619.

1

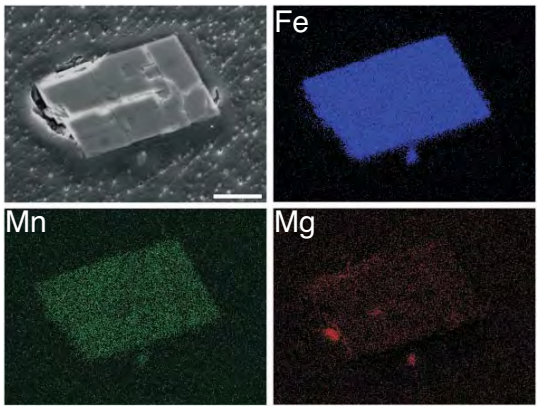

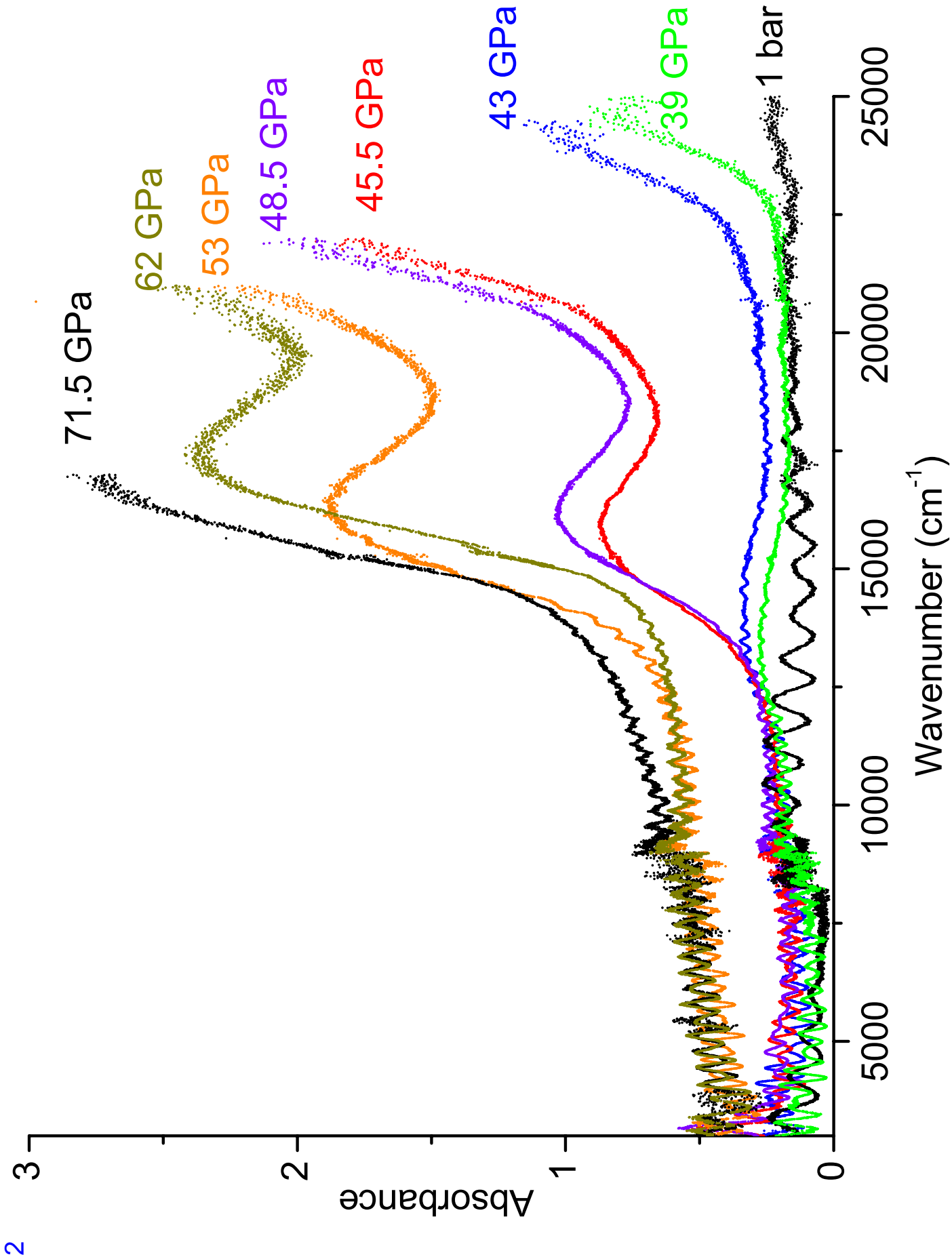

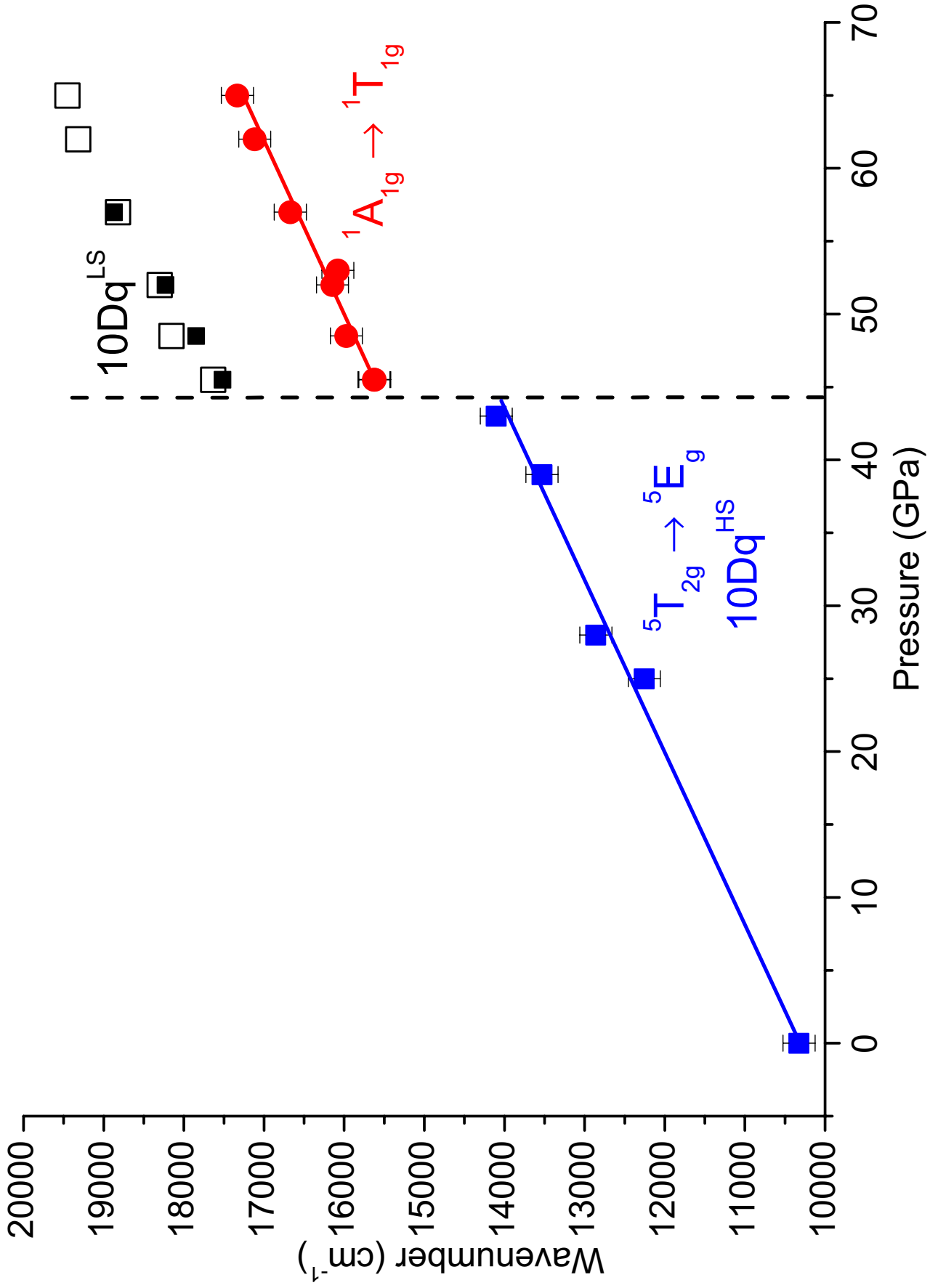
Wavenumber (cm-1)
20000
19000
18000
17000
16000
15000
14000
13000
12000
11000
10000
Pressure (GPa)
0
10
20
30
40
50
60
70
10Dq^LS
1A1g → 1T1g
5T2g → 5Eg
10Dq^HS

4

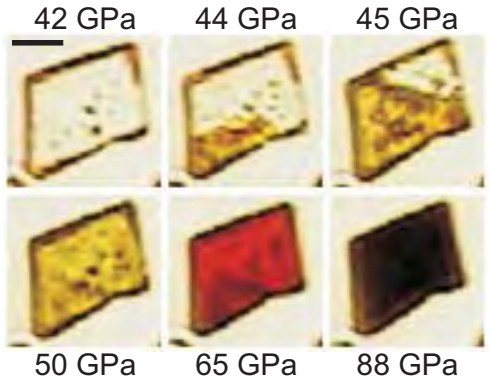

5

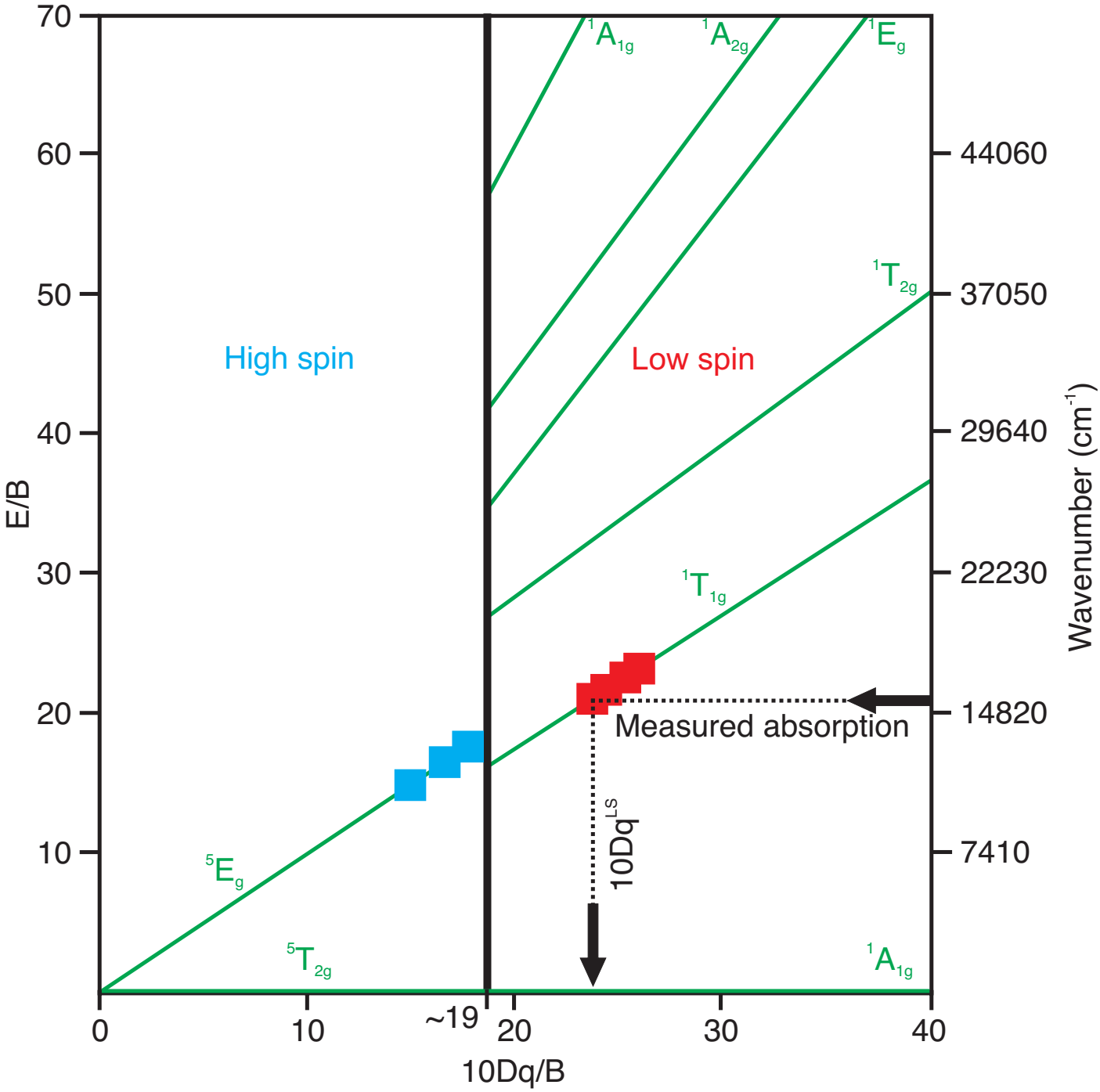
70
60
50
40
30
20
10
E/B
0
10
~19
20
30
40
10Dq/B
44060
37050
29640
22230
14820
7410
Wavenumber (cm-1)
1A1g
1A2g
1Eg
1T2g
1T1g
5Eg
5T2g
1A1g
High spin
Low spin
Measured absorption
10DqLS

6

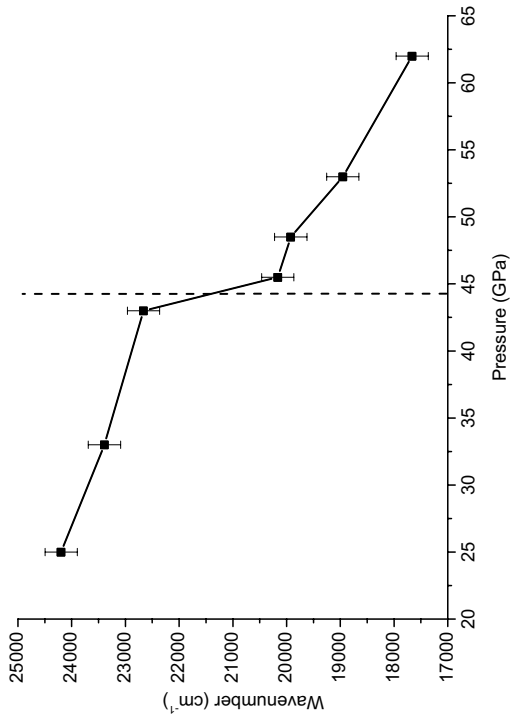
Pressure (GPa)
20
25
30
35
40
45
50
55
60
65
Wavenumber (cm-1)
25000
24000
23000
22000
21000
20000
19000
18000
17000